ELSEVIER

Journal of Nuclear Materials 275 (1999) 246–254

journal of nuclear materials

www.elsevier.nl/locate/jnucmat

Reactions of U–Zr alloy with Fe and Fe–Cr alloy

Kinya Nakamura[a], Takanari Ogata[a,*], Masaki Kurata[a], Akinori Itoh[b], Mitsuo Akabori[b]

[a] *Nuclear Fuel Cycle Department, Central Research Institute of Electric Power Industry, Iwato-kita 2-11-1, Komae-shi, Tokyo 201-8511, Japan*

[b] *Japan Atomic Energy Research Institute, Tokai-mura, Ibaraki-ken 319-1195, Japan*

Received 25 May 1999; accepted 24 August 1999

Abstract

The reaction zones formed in two kinds of diffusion couples: U–23at.%Zr/Fe and U–23at.%Zr/Fe–12at.%Cr, at 908, 923, 953, 973 and 988 K have been examined using the electron-probe microanalysis. In the U–Zr/Fe–Cr couples, diffusion of Cr to the U–Zr side is slower than that of Fe, and the Cr-rich phase is formed adjacent to the unreacted Fe–Cr alloy. Except for the Cr-rich phase, the measured compositions of the phases in the reaction zones in both U–Zr/Fe and U–Zr/Fe–Cr couples have corresponded well to those in the U–Zr–Fe ternary system. Each reaction zone can be divided to several layers. For the U–Zr side of the reaction zone, the configurations of the schematic diffusion paths, which are the curves connecting the average compositions of these layers on the U–Zr–(Fe + Cr) composition triangle, are independent of the annealing temperature and the Cr addition to Fe. For the Fe(–Cr) side, however, the paths depend on the annealing temperature and the Cr addition to Fe. Some of the phases that are expected to emerge considering the schematic diffusion path and the U–Zr–Fe phase diagram have not been found at 988 K.

PACS: 66.30.-h; 68.35.Fx; 81.30.Bx

1. Introduction

Uranium–plutonium–zirconium alloys have been considered one of the advanced fast reactor fuels. During irradiation, these alloys swell and come into contact with the cladding, then metallurgical reaction at the fuel-cladding interface occurs and affects the integrity of the cladding. The reaction between the fuel alloy and the Fe-base cladding materials should be well understood in order to evaluate the fuel performance.

Several studies were conducted on the reactions between U–Zr or U–Pu–Zr alloys and stainless steels [1–3]. The reactions in more fundamental systems, U–Zr alloys and Fe [4] were examined to understand the related reactions comprehensively. The phase relations in the U–Zr–Fe ternary alloys [5,6] were also studied to obtain a thermodynamic basis for the analysis of these reactions. In the present study, temperature dependency of the isothermal solid-state reactions in the U–23at.%Zr/Fe diffusion couple has been examined in the temperature range of 908–988 K. In addition, the reactions in the U–23at.%Zr/Fe–12at.%Cr couple have been investigated to understand the effects of the Cr addition to Fe on the reaction.

2. Experimental procedure

The U–23at.%Zr and Fe–12at.%Cr alloy ingots were prepared from the pure metals of U (99.9% purity), Zr (99.9%), Fe (99.995%), and Cr (99.99%) by arc-melting in a highly purified argon atmosphere on a water-cooled copper hearth. The arc-melted ingots were inverted and

* Corresponding author. Tel.: +81-3 3480 2111; fax: +81-3 3480 7956.

E-mail address: pogata@criepi.denken.or.jp (T. Ogata)

0022-3115/99/$ - see front matter
PII: S0022-3115(99)00227-5

re-melted; the inverting-melting cycle was repeated six times to enhance the homogeneity. Oxidation of the ingots during the fabrication process was minimized by arc-melting a pure Zr chunk before each melting cycle. The U–Zr alloy ingot was annealed at 1123 K for about 3 days to enhance its homogeneity, after being wrapped with tungsten foil and encapsulated in a quartz tube under an atmosphere of 0.025 MPa helium. The Fe–Cr alloy ingot was annealed at 1223 K for about 6 days in a similar manner. After annealing, each ingot was quenched by breaking the quartz tube in a water bath.

Samples of approximately $4 \times 4 \times 2$ mm^3 were taken from the homogenized alloy ingots and a pure Fe block. The diffusion couples consisting of U–Zr/Fe and U–Zr/Fe–Cr were assembled using these samples. The sample surface which would be the interface of the couple was polished with diamond paste right before assembling the couple. The diffusion couple was compressed in a stainless steel holder. The schematic view of the diffusion couple and the holder is illustrated in Fig. 1. The inside surface of the holder was lined with tantalum foils to prevent the couple from reacting with the holder. Each of the diffusion couple assemblies was encapsulated in a quartz tube under an atmosphere of 0.025 MPa helium, and annealed isothermally according to the conditions shown in Table 1. After annealing, the capsule was taken out of the furnace and quickly broken in a water bath so that the diffusion couple could be quenched rapidly. The annealed couple was cut perpendicularly to the interface. The cross section of the couple was ground and polished for the electron probe microanalysis (EPMA). The EPMA sample of the U–Zr/Fe couple annealed at 923 K in the previous study [4] was also prepared for the re-analysis. The compositions of the phases in the reaction layers were measured using the wavelength dispersive detector. The intensities of U-Mα (0.3910 nm), Zr-Lα (0.6071 nm), Fe-Kα (0.1936 nm), and Cr-Kα (0.2290 nm) X-rays were converted to the atomic fractions by the ZAF correction.

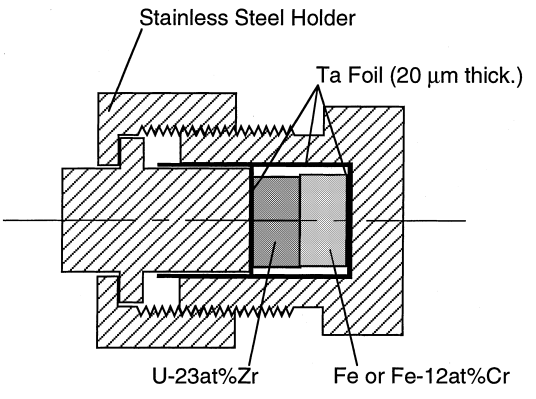

Fig. 1. Schematic view of the diffusion couple assembly.

Table 1
Diffusion annealing conditions

Diffusion couple	Temperature (K)	Annealing time (ks)
U–23at.%Zr/Fe	908	598
		1181
	923	922
		1465
		2995
	973	144
		346
		1206
	988	346
		1206
U–23at.%/ Fe–12at.%Cr	953	1206
	973	346
		1206
	988	144

3. Results

3.1. U–Zr/Fe couples

Back-scattered electron images of the reaction zones for the U–Zr/Fe couples annealed at 923, 973, and 988 K

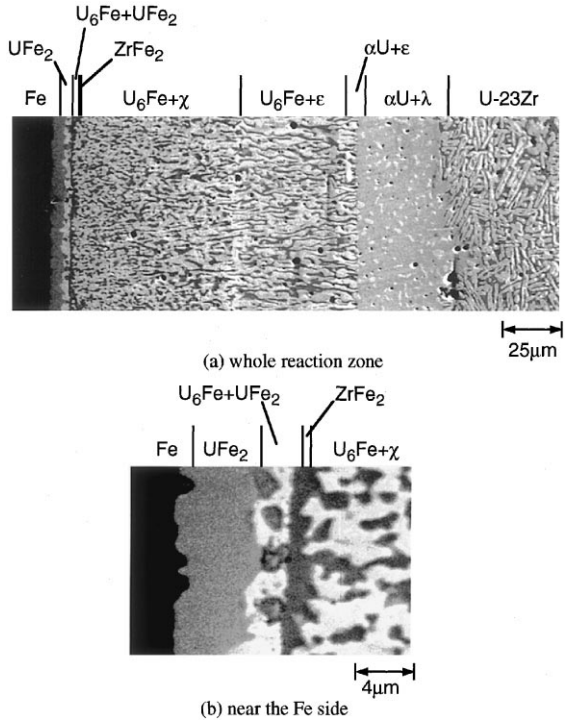

Fig. 2. Back-scattered electron images of the reaction zone for the U–23at.%Zr/Fe couple annealed at 923 K: (a) whole reaction zone and (b) near the Fe side.

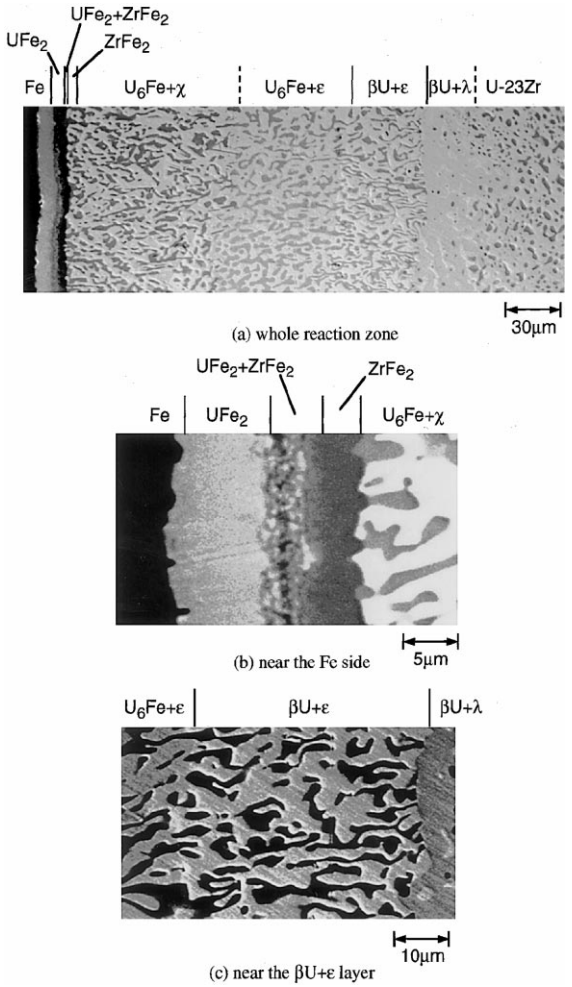

Fig. 3. Back-scattered electron images of the reaction zone for the U–23at.%Zr/Fe couple annealed at 973 K: (a) whole reaction zone; (b) near the Fe side and (c) near the $\beta U + \varepsilon$ layer.

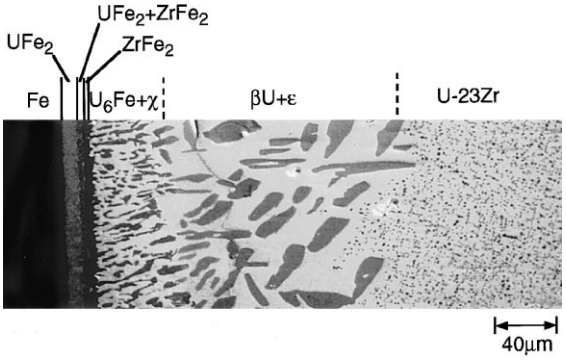

Fig. 4. Back-scattered electron image of the reaction zone for the U–23at.%Zr/Fe couple annealed at 988 K.

are shown in Figs. 2–4, respectively. The structure of the reaction zone for 908 K, which is not presented here, is essentially the same as that for 923 K. The measured compositions of the phases formed in the reaction zone are consistent with those in the U–Zr–Fe phase diagrams, which has been determined experimentally at 853, 973, and 1073 K [6] and optimized using a thermodynamic assessment [5,6]. Each reaction zone can be divided into several layers, as indicated in Figs. 2–4. Some of the layers have shown structures too minute for the quantitative microanalysis: for example, the two-phase layer between the UFe_2 and the $ZrFe_2$ single-phase layers in Fig. 3. In such cases, the phase compositions have been estimated from the back-scattered electron images, the X-ray mapping for each element, and the U–Zr–Fe isotherms calculated at respective temperatures. The identified or estimated phases in the layers are summarized in Table 2, and also indicated in Figs. 2–4. The χ, ε, and λ phases in the figures and tables are the ternary compounds, the compositions of which are U–32Zr–50Fe, U–(33–50)Zr–33Fe, and U–(21–

Table 2
Phases in the reaction zones in the U–23at.%Zr/Fe couples

Diffusion couple	U–23at.%Zr/Fe			
Temperature (K)	908	923	973	988
Unreacted Fe	αFe	αFe	αFe	αFe
Layers	UFe_2	UFe_2	UFe_2	UFe_2
	$U_6Fe + UFe_2$	U_6Fe_2		
			$U_6Fe_2 + ZrFe_2$	$U_6Fe_2 + ZrFe_2$
	$ZrFe_2$	$ZrFe_2$	$ZrFe_2$	$ZrFe_2$
	$U_6Fe + \chi$	$U_6Fe + \chi$	$U_6Fe + \chi$	$U_6Fe + \chi$
	$U_6Fe + \varepsilon$	$U_6Fe + \varepsilon$	$U_6Fe + \varepsilon$	
	$\alpha U + \varepsilon$	$\alpha U + \varepsilon$	$\beta U + \varepsilon$	$\beta U + \varepsilon$
	$\alpha U + \lambda$	$\alpha U + \lambda$	$\beta U + \lambda$	
Unreacted U–Zr	$\alpha U + \gamma_2$	$\alpha U + \gamma_2$	$\gamma_1 + \gamma_2$	$\gamma_1 + \gamma_2$

Note: UFe_2 and U_6Fe phases include <3at.%Zr and <2at.%Zr, respectively. $ZrFe_2$ phase includes ~10at.%U.

25)Zr–6Fe (in at.%), respectively [6]. The two-phase layers of αU + ε and U_6Fe + χ could not be distinguished clearly in the previous study on the U–Zr/Fe couple annealed at 923 K [4]. In the present study, however, these layers have been identified as indicated in Fig. 2 and Table 2 by adjusting the contrast of the electron images and tuning the electron beam more carefully.

The average compositions of the two-phase layers have not been measured directly, but can be estimated from the phase compositions and areal fractions of each phase in the electron images. Fig. 5 shows the schematic plots of the average compositions of the layers on the calculated U–Zr–Fe isotherms at respective temperatures. In the calculation of these isotherms, the ε-phase has been assumed to be a stoichiometric compound for simplicity, and the solubilities of Zr in UFe_2, U in $ZrFe_2$, and Zr in U_6Fe have been ignored [5,6]. It should be noted that in the calculated isotherms, narrow two-phase regions exist between three-phase regions (indicated by solid bold lines) although they are buried in the neighboring bold lines. The dotted gray lines in Fig. 5 connecting the average compositions of the layers are

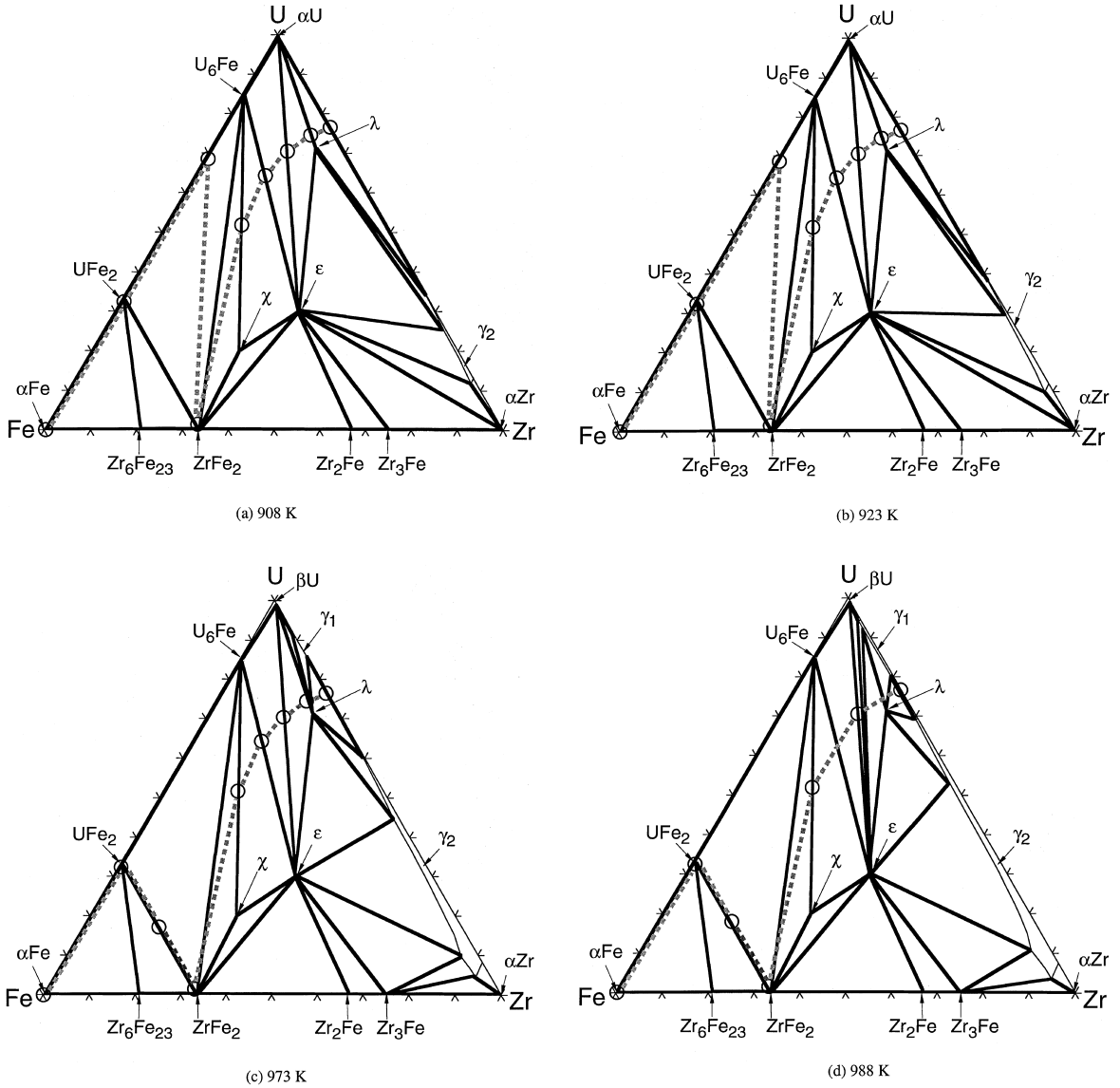

Fig. 5. The schematic diffusion paths (dotted gray lines) for the U–23at.%Zr/Fe couples annealed at: (a) 908 K; (b) 923 K; (c) 973 K and (d) 988 K drawn on the calculated U–Zr–Fe isotherms at the respective temperatures. Open circles indicate approximate average compositions of the layers.

Table 3
Phases in the reaction zones U–23at.%Zr/Fe–12at.%Cr couples

Diffusion couples	U–23at.%Zr/Fe–12at.%Cr		
Temperature (K)	953	973	988
Unreacted Fe–Cr	Solid solution	Solid solution	Solid solution
Layers	Cr-rich layer	Cr-rich layer	Cr-rich layer
	UFe_2	UFe_2	UFe_2
	U_6Fe	U_6Fe	U_6Fe
	$U_6Fe + ZrFe_2$	$U_6Fe + ZrFe_2$	$U_6Fe + ZrFe_2$
	$U_6Fe + \chi$	$U_6Fe + \chi$	
	$U_6Fe + \varepsilon$	$U_6Fe + \varepsilon$	U6Fe + ε
	$\beta U + \varepsilon$	$\beta U + \varepsilon$	$\beta U + \varepsilon$
	$\beta U + \lambda$	$\gamma_1 + \lambda$	$\gamma_1 + \lambda$
Unreacted U–Zr	$\beta U + \lambda_2$	$\gamma_1 + \gamma_2$	$\gamma_1 + \gamma_2$

Note: UFe_2 and U_6Fe phases include < 3at.%Zr and < 2at.%Zr, respectively. $ZrFe_2$ phases includes ~10at.%U. Cr Contents in the phases listed above are as follows: U_6Fe: ~1at.%, UFe_2: ~10at.%, $ZrFe_2$: ~10–20at.%, χ : ~3at.%, not detected in ε, βU, γ, and λ.

called 'schematic diffusion paths' in the present report. The structure of the reaction zone can be illustrated by the schematic diffusion path drawn on the phase diagram. The configurations of the schematic diffusion paths for the U–Zr side of the reaction zone are similar to each other. The only difference among the path configurations is found near the edges of the three-phase region of $U_6Fe + UFe_2 + ZrFe_2$; the path goes through the two-phase region of $U_6Fe + UFe_2$ at 908 and 923 K, but through the $UFe_2 + ZrFe_2$ region at 973 and 988 K. In the reaction zone for 973 K (Figs. 3 and 5(c)), the $\gamma_1 + \lambda$ layer has not been distinguished from the $\beta U + \lambda$ layer. It is possible that the $\gamma_1 + \lambda$ layer actually exists but its detection has been missed because of the similarity between the compositions of the γ_1 and the βU phases. The $U_6Fe + \varepsilon$, $\gamma_1 + \varepsilon$ and $\gamma_1 + \lambda$ layers can be expected to emerge at 988 K, comparing the schematic diffusion path to the calculated isotherm (Fig. 5(d)). However, they have not been found (Figs. 4 and 5(d)).

3.2. U–Zr/Fe–Cr couples

Fig. 6 shows a back-scattered electron image of the reaction zone in the U–Zr/Fe–Cr couple annealed at 973 K. The enlarged image of the Fe–Cr side of the reaction zone is shown in Fig. 7(a) with the element mapping results (Fig. 7(b)–(e)). The images in Fig. 7 indicate that diffusion of Cr to the U–Zr side is slower than that of Fe; Cr is left in the Fe–Cr side of the reaction zone and the Cr-rich phase is formed adjacent to the unreacted Fe–Cr alloy. Chromium has been detected in the UFe_2, $ZrFe_2$, and χ phases, but not in U_6Fe, ε, λ, βU, and γ_1 phases. The Cr-rich phase has been formed in all the U–Zr/Fe–Cr couples, independent of the annealing temperature. While the composition of the Cr-rich phase has not been determined, it is presumably the σ-phase of the Fe–Cr binary system considering the element mapping results in Fig. 7 and the results for the U–23at.%Zr/stainless-steel couples reported in Ref. [2]. Except for the Cr-rich phase, the phase compositions measured for all the U–Zr/Fe–Cr couples have corresponded well to those in the U–Zr–Fe system when the sum of the concentrations of Fe and Cr is regarded as the Fe concentration. The phases identified or estimated in the manner described in Section 3.1 are summarized in Table 3, and also indicated in Figs. 6 and 7. The single-phase layer of U_6Fe is formed in all the U–Zr/Fe–Cr couples, while it has not been observed in the U–Zr/Fe couples.

Based on the similarity between the phases for the U–Zr/Fe and the U–Zr/Fe–Cr couples, the average compositions of the layers in the U–Zr/Fe–Cr reaction zones are schematically plotted on the U–Zr–Fe composition tri-

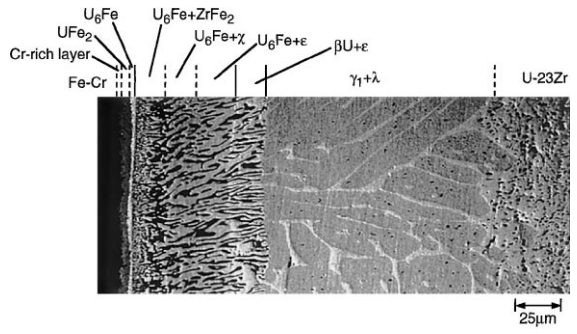

Fig. 6. Back-scattered electron image of the reaction zone for the U–23at.%Zr/Fe–12at.%Cr couple annealed at 973 K.

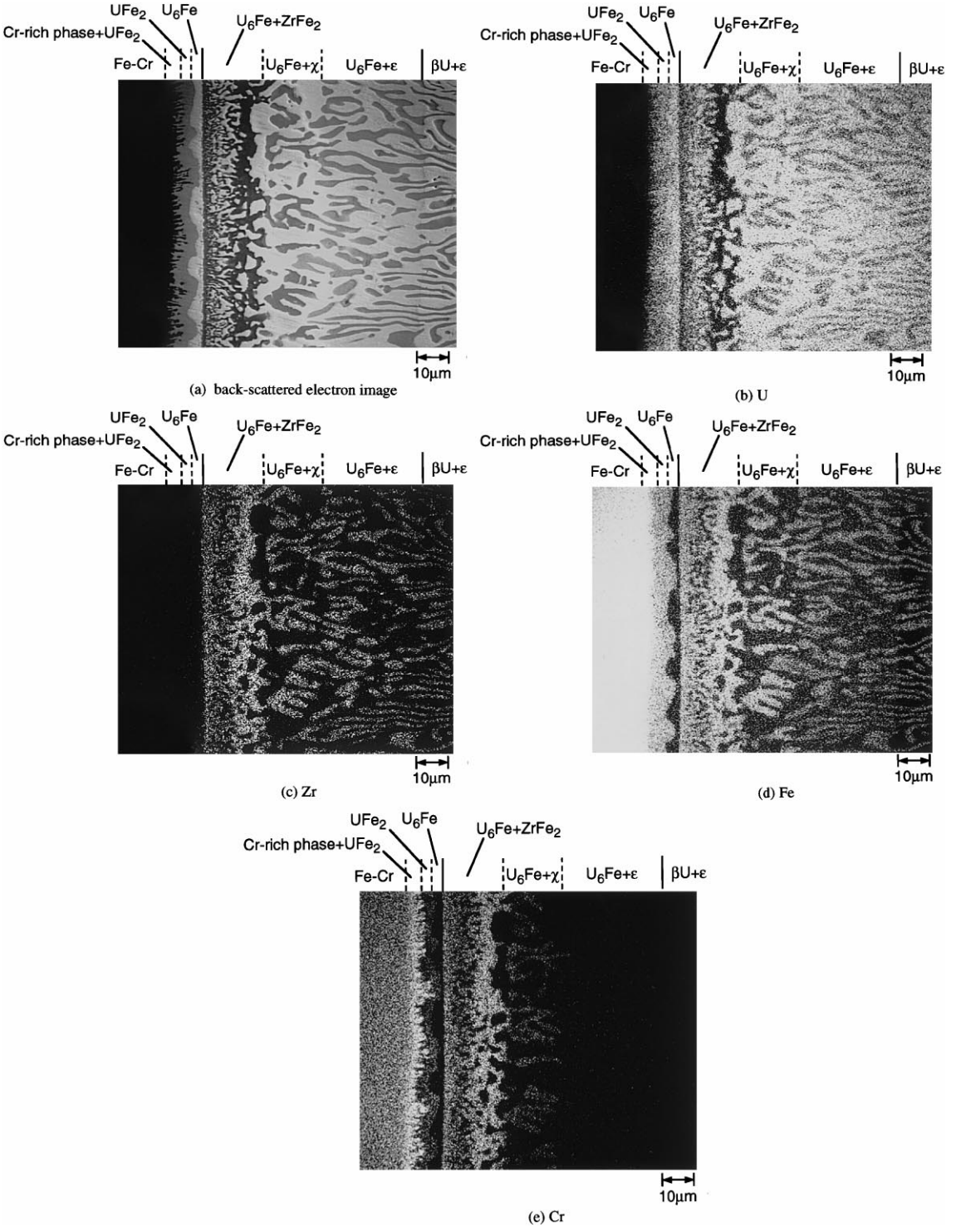

Fig. 7. Fe–Cr side of the reaction zone for the U–23at.%Zr/Fe–12at.%Cr couple annealed at 973 K: (a) back-scattered electron image and element mappings for (b) U; (c) Zr; (d) Fe and (e) Cr.

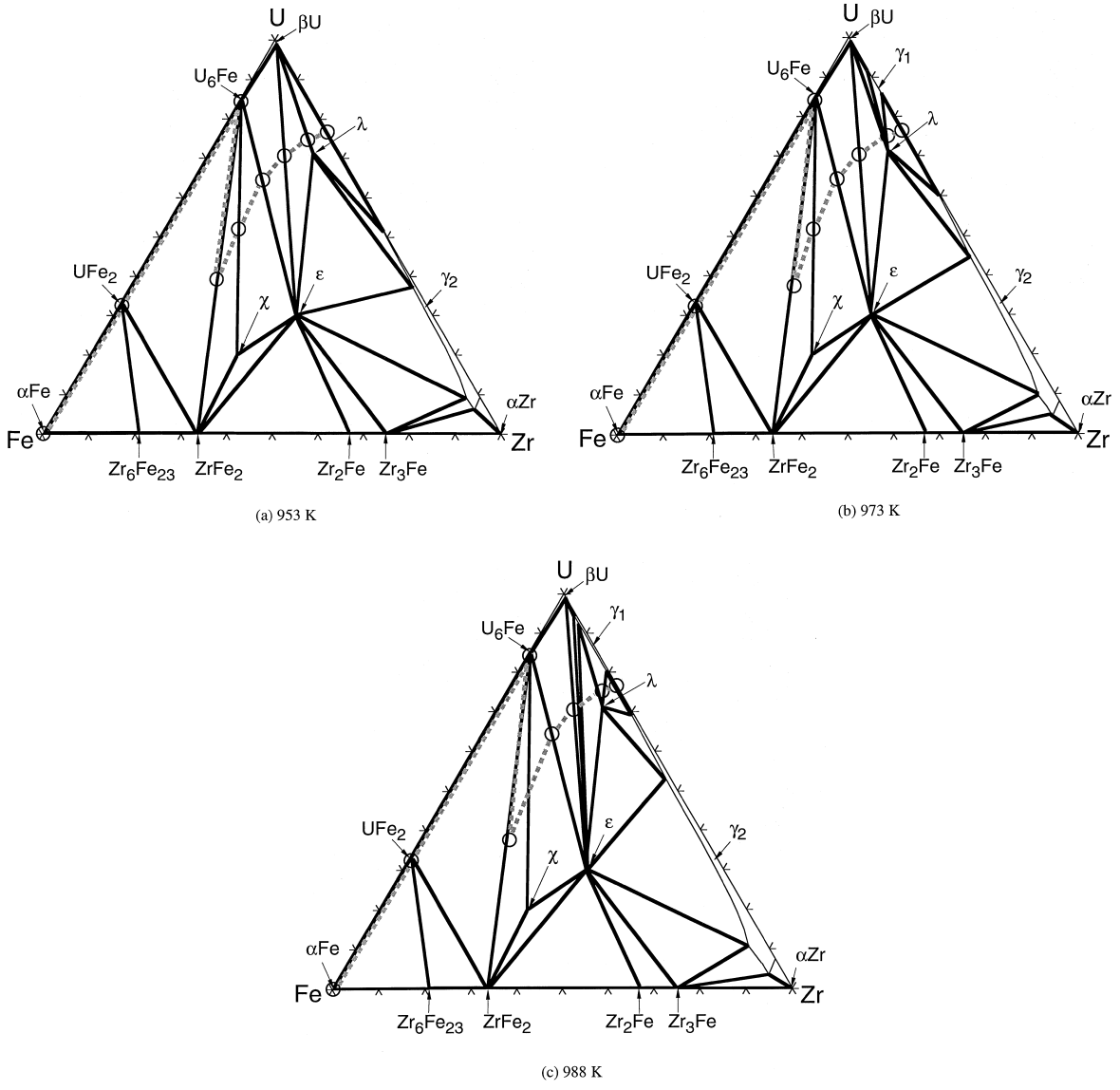

Fig. 8. The schematic diffusion paths (dotted gray lines) for the U–23at.%Zr/Fe–12at.%Cr couples annealed at: (a) 953 K; (b) 973 K and (c) 988 K drawn on the calculated U–Zr–Fe isotherms at the respective temperatures. Open circles indicate approximate average compositions of the layers. The sum of the concentrations of Fe and Cr is taken as one concentration variable. The Cr-rich layer is excluded from the plots.

angle (Fig. 8(a)–(c)), taking the sum of the concentrations of Fe and Cr as one concentration variable. The layer including the Cr-rich phase is excluded from the plots. The calculated U–Zr–Fe isotherms at respective temperatures are also drawn in Fig. 8. The dotted gray lines in the figure connecting the average compositions of the layers are the schematic diffusion paths for the U–Zr/Fe–Cr couples. The configurations of the schematic diffusion paths are similar to each other. The existence of the $\beta U + \lambda$ layer at 973 K is ambiguous (Fig. 6), as is the case for the $\gamma_1 + \lambda$ layer in the U–Zr/Fe couples annealed at 973 K. The two-phase layers of $U_6Fe + \chi$ and $\gamma_1 + \varepsilon$ have not been found at 988 K, although they can be expected to appear considering the schematic diffusion path and the calculated isotherm (Fig. 8(c)).

3.3. Growth of reaction zones

Thicknesses of the reaction zones are plotted against the square root of the annealing time, t, in Fig. 9. The reaction zone thickness grows approximately in proportion to $t^{1/2}$. It means that the reaction in the U–Zr/

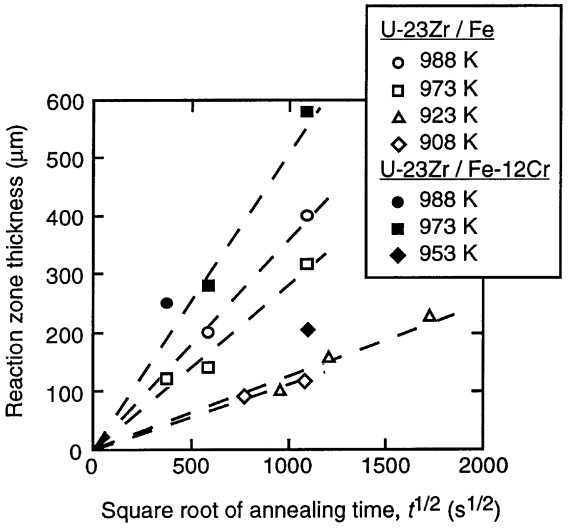

Fig. 9. Growth of the reaction zones.

Fe(–Cr) couples is diffusion-controlled. Comparing the growth rates for the annealing temperatures of 973 and 988 K, Cr addition to Fe seems to increase slightly the rate of the reaction between U–Zr and Fe.

4. Discussion

The configurations of the schematic diffusion paths for the U–Zr side of the reaction zone, from the $U_6Fe + \chi$ layer to the unreacted U–Zr end, are similar to each other and independent of the annealing temperature and the Cr addition to Fe, as stated above. This can be understood based on the result that Cr does not diffuse deeply to the U–Zr side, and also from the fact that the phase relations in the U–Zr–Fe system [6] do not change in the temperature range of 908–988 K, except for the phase transition near the U–Zr edge. For the Fe(–Cr) side of the reaction zone, however, the schematic diffusion paths along the edges of the $U_6Fe + UFe_2 + ZrFe_2$ three-phase region depend on the annealing temperature and the Cr addition. While the causes of these variations in the paths cannot be explained clearly at this stage, one of the possible explanations may be provided by considering variations of the formation energies of the U_6Fe, UFe_2, and $ZrFe_2$ phases with temperature and Cr content. The changes in the diffusivities of the elements may also affect the phase structure in the reaction zone.

Another noticeable point is the absence of some of the phases that are expected to emerge considering the schematic diffusion path and the U–Zr–Fe phase diagram. It has occurred particularly at 988 K; the absent layers are the $U_6Fe + \varepsilon$, $\gamma_1 + \varepsilon$ and $\gamma_1 + \lambda$ layers in the U–Zr/Fe couple (Figs. 4 and 5(d)), and the $U_6Fe + \chi$ and $\gamma_1 + \varepsilon$ layers in the U–Zr/Fe–Cr couple (Fig. 8(c)). Taking account of the small differences between the Gibbs free energies of the γ_1 and βU phases [5], there is a possibility that the $\beta U + \gamma_1 + \lambda$ three-phase region may exist in the U–Zr–Fe isotherm at 988 K instead of the $\gamma_1 + \varepsilon$ two-phase region (Fig. 5(d) and Fig. 8(c)). In this case, the isotherm at 988 K would be close to that at 973 K, and the absence of the $\lambda_1 + \varepsilon$ layer in both types of couples would be reasonable. In any case, the schematic diffusion path at 988 K must cross the tie-line(s) extending from the λ phase, so that the λ phase is expected to emerge in the reaction zone at 988 K. Also the absences of the $U_6Fe + \varepsilon$ for the U–Zr/Fe couple and the $U_6Fe + \chi$ for the U–Zr/Fe–Cr couple cannot be attributed to the above-mentioned uncertainty in the thermodynamic assessment. The cause of this kind of phase absence was explained by Philibert [7] for a binary diffusion couple; once a phase is formed, it is possible that the Gibbs free energy driving the next phase formation becomes very small. A similar explanation may be applicable to the phase absence in the present U–Zr/Fe (–Cr) couples, as follows. As for the λ phase, for example, it decomposes to ε and γ phases at 999 K [6]. At 988 K, only 11 K below the decomposition temperature, the Gibbs free energy of the λ phase formation is close to that of mixing of the γ (or $\gamma_1 + \gamma_2$) and ε phases. The energy driving the λ phase formation will be, therefore, insufficient after the ε phase is formed adjacent to the unreacted U–Zr alloy (two-phase of $\gamma_1 + \gamma_2$ at 988 K). Consequently, the λ phase has not emerged in the U–Zr/Fe couples at 988 K.

Note that the λ phase has emerged in all the U–Zr/Fe–Cr couples, and also that the χ phase is absent only in the U–Zr/Fe–Cr couple annealed at 988 K. These results seem to be inconsistent with the immobility of Cr in the present system. In order to understand the mechanism of the absence of these phases in the U–Zr/Fe–Cr couples, assessments of the thermodynamics of the U–Zr–Fe–Cr quaternary system and the diffusivities of the elements in the relevant phases will be required.

5. Conclusion

Two kinds of diffusion couples: U–23at.%Zr/Fe and U–23at.%Zr/Fe–12at.%Cr, have been annealed isothermally in the temperature range of 908–988 K. The reaction zones in those couples have been examined. The results are summarized as follows:

1. The reactions in the U–Zr/Fe(–Cr) couples are diffusion-controlled.
2. In the U–Zr/Fe–Cr couples, the diffusion of Cr to the U–Zr side is slower than that of Fe, and the Cr-rich

phase is formed adjacent to the unreacted Fe–Cr alloy.

3. Except for the Cr-rich phase, the measured compositions of the phases in the reaction zones in the U–Zr/Fe(–Cr) couples have corresponded well to those in the U–Zr–Fe ternary system.
4. The configurations of the schematic diffusion paths for the U–Zr side of the reaction zone are similar to each other, independent of the annealing temperature and the Cr addition to Fe.
5. For the Fe(–Cr) side of the reaction zone, the schematic diffusion paths along the edges of the $U_6Fe + UFe_2 + ZrFe_2$ three-phase region depend on the annealing temperature and Cr addition to Fe. Some of the phases which are expected to emerge considering the schematic diffusion path and the U–Zr–Fe phase diagram have not been found at 988 K. The assessments of the thermodynamics of the U–Zr–Fe–Cr quaternary system and the diffusivities of the elements in the relevant phases will be required in order to explain the causes of the variations in the schematic diffusion paths and the absence of these phases.

Acknowledgements

The authors appreciate valuable discussions with Dr T. Ogawa of the Japan Atomic Energy Research Institute and Mr T. Yokoo of the Central Research Institute of Electric Power Industry.

References

[1] D.D. Keiser Jr., M.A. Dayananda, J. Nucl. Mater. 200 (1993) 229.
[2] D.D. Keiser Jr., M.A. Dayananda, Metall. Mater. Trans. 25A (1994) 1649.
[3] D.D. Keiser Jr., M.C. Petri, J. Nucl. Mater. 240 (1996) 51.
[4] T. Ogata, M. Kurata, K. Nakamura, A. Itoh, M. Akabori, J. Nucl. Mater. 250 (1997) 171.
[5] M. Kurata, T. Ogata, K. Nakamura, T. Ogawa, J. Alloys Comp. 271–273 (1998) 636.
[6] K. Nakamura, M. Kurata, T. Ogata, A. Itoh, M. Akabori, to be published in J. Nucl. Mater.
[7] J. Philibert, Def. Diffus. Forum 66–69 (1989) 995.